
 Cite this: *RSC Adv.*, 2023, **13**, 10914

# Cocrystal of phloretin with isoniazid: preparation, characterization, and evaluation†

 Zhongyu Lu,<sup>a</sup> Hankun Chen,<sup>b</sup> Jiaxin Mo,<sup>a</sup> Xiaohong Yuan,<sup>a</sup> Dawei Wang,<sup>c</sup> Xianhui Zheng<sup>a</sup> and Wei Zhu<sup>\*,a</sup>

Phloretin (Phl) is a natural flavonoid compound with wide range of biological activities but demonstrates poor water solubility and limited pharmacological effects. In this study, one cocrystal of phloretin–isoniazid (Phl–Inz) was prepared successfully using the solvent evaporation method. The physical properties of cocrystal were characterized by differential scanning calorimetry (DSC), thermogravimetric analysis (TG), powder X-ray diffraction (PXRD), Fourier-transform infrared (FT-IR) and single crystal X-ray diffraction (SCXRD). The Hirshfeld surface analysis explained further interactions in the cocrystal. The solubility test showed that the solubility of the cocrystal was increased at pH 1.2 and pH 6.8 compared to that of the pure drug. The test *in vitro* simulated gastrointestinal digestion showed that the release of phloretin in the cocrystal was better than that in the pure phloretin. The results of the DPPH and ABTS scavenging activity showed that the *in vitro* antioxidant activity of the cocrystal was improved. The anticancer assay exhibited improved cytotoxicity in the Phl–Inz cocrystal as compared with the pure Phl.

Received 4th February 2023

Accepted 14th March 2023

DOI: 10.1039/d3ra00750b

[rsc.li/rsc-advances](https://rsc.li/rsc-advances)

## Introduction

Phloretin (Phl) is a kind of plant polyphenol formed by the skeleton structure of C<sub>6</sub>–C<sub>3</sub>–C<sub>6</sub> (two aromatic rings connected by the C<sub>3</sub> chain)<sup>1,2</sup> (Fig. 1). Recent studies have shown that phloretin demonstrates various pharmacological effects, such as antioxidant activity,<sup>3</sup> immunosuppression,<sup>4</sup> and antimicrobial<sup>5</sup> and anticancer<sup>6</sup> activities. However, Phl belongs to the biopharmaceutics classification system (BCS) class II, which is characterized by low solubility and high permeability, and its low solubility limits the full play of its pharmacological effects.<sup>7–9</sup>

In recent years, pharmaceutical cocrystal technology has become a research hotspot to improve solubility, dissolution, bioavailability, and other properties of drugs.<sup>10–13</sup> This technology did not change the molecular structure of drugs but only changed the physical and chemical properties of drugs through intermolecular forces, providing a new way for the development of poorly water-soluble drugs.<sup>14,15</sup> Pharmaceutical cocrystal refers to the crystal formed by two or more kinds of molecules bonded in the same lattice by non-covalent bonds based on a fixed stoichiometric ratio.<sup>16</sup> The components of

pharmaceutical cocrystals include one or more active pharmaceutical ingredients (APIs) and one or more cocrystal formers (CCFs).<sup>17</sup> A cocrystal is a supramolecular complex formed by API and CCF. The intermolecular forces for cocrystals include hydrogen bonding, halogen bonding, van der Waals force and  $\pi$ –bonding, among which hydrogen bonding is the most important intermolecular force for cocrystal formation between API and CCF.<sup>18–20</sup> These intermolecular forces reshape the structure of the cocrystal, which can change the dissolution behaviour of the cocrystal.

Therefore, pharmaceutical cocrystal was used to improve the solubility of Phl. According to the literature,<sup>7,21–24</sup> the ratio of Phl and its similar structure to co-former is usually 1 : 1 in cocrystal, which was chosen as the ratio of Phl and co-former in this experiment. Water-soluble isoniazid (Inz) was chosen as a co-former to prepare cocrystal with Phl and Phl–Inz cocrystal was successfully obtained by the solvent evaporation method. Phl and other co-formers were unsuccessfully synthesized into

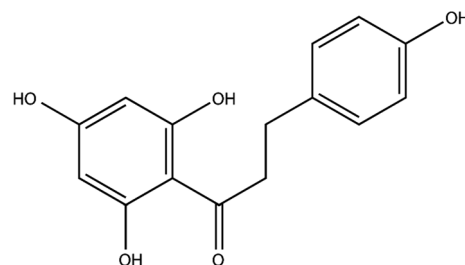


Fig. 1 Chemical structure of Phl.

<sup>a</sup>The Second Clinical College of Guangzhou University of Chinese Medicine, Guangzhou University of Chinese Medicine, Guangzhou, China. E-mail: lzy971012@163.com; zhuwei9201@163.com

<sup>b</sup>Research and Development Department, Guangzhou Qinglan Biotechnology Company Limited, Guangzhou, China

<sup>c</sup>ShunDe Hospital, Guangzhou University of Chinese Medicine, Foshan, China

 † CCDC 2239405. For crystallographic data in CIF or other electronic format see DOI: <https://doi.org/10.1039/d3ra00750b>


cocrystals or formed mixtures of cocrystal and API. The cocrystal's structure was determined by differential scanning calorimetry-thermogravimetry (DSC-TG), Fourier-transform infrared (FT-IR), nuclear magnetic resonance ( $^1\text{H}$  NMR), powder X-ray diffraction (PXRD), and single-crystal X-ray diffraction (SCXRD). Compared with PhI, the release in gastrointestinal fluid, solubility and anticancer activities of PhI-Inz were improved.

## Materials and methods

### Materials

Phloretin (PhI, purity  $\geq 98\%$ ), isoniazid (Inz, purity = 98%), 2-picolinic acid (99%), theophylline (99%), 4-aminobenzamide (98%), proline (99%), nicotinic acid (99%) and 4-picolinic acid (99%) were purchased from Shanghai Macklin Biochemical Co., Ltd (Shanghai, China). Phloretin (HPLC  $\geq 98\%$ ) and maleic (99%) acid were purchased from Shanghai Yuanye Bio-Technology Co., Ltd. (Shanghai, China). 2,2'-Azino-bis(3-ethylbenzothiazoline-6-sulfonic acid) diammonium salt (ABTS) was purchased from Sigma Life Science (St. Louis, MO, USA). 1,1-Diphenyl-2-picrylhydrazyl (DPPH) was purchased from Shanghai Macklin Biochemical Co., Ltd. (Shanghai, China). Methanol was obtained from Guangzhou Reagent Co., Ltd. (Guangzhou, China). The A549 cell line and HepG2 cell line were purchased from the Institute of Biochemistry and Cell Biology Sciences, Chinese Academy of Sciences (Shanghai, China).

### Powder X-ray diffraction (PXRD)

The generation of new crystalline phases leads to the disappearance of all or part of the characteristic peaks of API or CCF and the appearance of new peaks of cocrystal. The PXRD measurements of PhI, co-formers and cocrystals were tested using an X'pert multifunctional powder X-ray diffractometer (PANalytical, Holland) operated with Cu K $\alpha$  radiation ( $\lambda = 1.540598 \text{ \AA}$ ) at 30 mA and 40 kV. The XRD patterns of all samples were collected over an angle of 3–40° with a scan step size of 0.0131° per step and scan speed of 15° min $^{-1}$  at 25–26 °C.

### Preparation and screening of phloretin cocrystal

The binary cocrystal was formed with PhI and co-former, which were dissolved in methanol at a 1 : 1 mol ratio. The co-formers were chosen from isoniazid, 2-picolinic acid, theophylline, 4-aminobenzamide, proline, maleic acid, nicotinic acid and 4-picolinic acid. The two solutions were mixed and stirred in closing bottles of a parallel synthesizer and sonicated to complete dissolution. After stirring for 12 h at room temperature, the solution was transferred to a beaker and evaporated slowly. The crystals were obtained from the solution after 3–5 days and dried under vacuum at 45 °C for 8 h. The disappearance and appearance of diffraction peaks could determine whether the cocrystal was formed successfully. The samples were identified by PXRD to analyse the diffraction peak of mixtures for cocrystal screening.

### Thermal test

The melting point and thermal behaviour of samples were tested by DSC/DTA-TG STA 449 F5 Jupiter® (NETZCH, Germany) instrument. Approximately 4–6 mg of samples (PhI, co-formers and cocrystals) were placed in an aluminum pan and analysed from 30 °C to 500 °C with a rate of 10 °C min $^{-1}$ . N $_2$  was used as purge gas and protect gas.

### Fourier-transform infrared (FT-IR)

FT-IR studies were conducted using a Fourier-Transform Infrared Spectrometer (PerkinElmer, United States). The tested samples were dried in a vacuum drying oven at 45 °C for 6 h before testing, and the data were collected over the range of 4000–400 cm $^{-1}$  and processed by spectrum software (PerkinElmer).

### Nuclear magnetic resonance analysis ( $^1\text{H}$ NMR)

All  $^1\text{H}$  NMR spectra of the cocrystal were recorded using DMSO- $d_6$  with TMS as an internal standard at room temperature on a 600 MHz nuclear magnetic resonance spectrometer (Bruker, Germany). All spectra were processed on MestReNova.

### Single crystal X-ray diffraction analysis (SCXRD)

The crystallographic data of the PhI-Inz cocrystal were collected using an Agilent SuperNova diffractometer with Cu K $\alpha$  radiation ( $\lambda = 1.5418 \text{ \AA}$ ) at 150 K. Data reduction and absorption correction were processed using the CrysAlis<sup>Pro</sup>. The structure of the cocrystal was solved by direct methods using Olex2 ShelXT<sup>25</sup> and ShelXL<sup>26</sup> (CCDC number: 2239405†). The figures were drawn using Mercury or Olex2.

### Hirshfeld surfaces and 2D fingerprint plots

Hirshfeld surface analysis was used to investigate the structure of the PhI-Inz cocrystal. Hirshfeld surface and molecular fingerprints of PhI-Inz cocrystal using Crystal-Explorer 21.5.<sup>27</sup>

### High-performance liquid chromatography (HPLC)

The concentration of PhI was determined by HPLC using Agilent 1200 (Agilent, America) systems equipped with an Agilent G1311A pump and an Agilent G1315D DAD. The separation was carried out using a Diamonsil C18 column (250 mm  $\times$  4.6 mm, 5  $\mu\text{m}$ ) with a flow rate of 1 mL min $^{-1}$  at 30 °C. The mobile phases were composed of solution A (water) and solution C (acetonitrile), and the gradient elution was set as follows: 40–60% C (0–12 min) and 60–40% C (12–15 min). The injection volume was 15  $\mu\text{L}$ , and the detection wavelength was 273 nm.

### Solubility experiments

The solubility of PhI and its cocrystal were measured by applying the shake-flask method in a pH 1.2  $\pm$  0.2 hydrochloric acid buffer and pH 6.8  $\pm$  0.2 phosphate buffer solution, which was described in the literature with slight modification.<sup>7</sup> An excess amount of mixture (containing 50 mg PhI), PhI or PhI-Inz cocrystal were sieved through 100-mesh sieves and added into



a penicillin bottle containing 10 mL solution, and the resulting suspension was rotated at 100 rpm for 24 h at  $37 \pm 0.5$  °C. Sampling intervals were fixed at 5, 10, 15, 20, 30, 45, 60, 75, 90, 120, 180, 240, 300, 360, 420, 540, 720, and 1440 min with 0.4 mL aliquots withdrawn and replaced with an equal amount of buffer. The samples were centrifuged at 5000 rpm for 5 min and filtered through 0.22  $\mu\text{m}$  nylon filters for HPLC analysis ( $n = 3$ ) using the methods described in HPLC.

### *In vitro* simulated gastrointestinal digestion

To explore the kinetics of drug release in gastrointestinal fluid, the kinetic release profile of phloretin from cocrystals was studied in simulated gastric fluid (SGF) and Simulated Intestinal Fluid (SIF). The detection of *in vitro* simulated gastrointestinal digestion was modified based on the method documented in the literature.<sup>28</sup> About 6 mg of Phl–Inz cocrystal was placed in 4 mL of SGF release medium and stirred at 37 °C for 2 h. After that, the pH of SGF was adjusted to pH 6.8 and mixed with SIF release medium at a ratio of 1 : 1 (v/v) and stirred at 37 °C for 4 h. Every 30 min during the simulated digestion process, 0.8 mL of the mixture was collected, and 0.8 mL of fresh release medium was replenished to maintain the same volume. The concentration of phloretin in the collected mixture was determined by HPLC ( $n = 3$ ) using the methods described in HPLC.

### *In vitro* antioxidant activity

**DPPH free radical-scavenging activity.** The detection of DPPH free radical scavenging ability was modified based on the method documented in the literature.<sup>29</sup> 1 mL of DPPH alcoholic solution (0.2 mmol L<sup>-1</sup>), and 1 mL of sample (containing concentrations of 20, 40, 60, 80, 100  $\mu\text{g mL}^{-1}$  in methanol) was mixed in a test tube, shaken evenly and incubated for 30 min at room temperature in a dark place. After the reaction, the absorbance was measured at a wavelength of 517 nm.

**ABTS free radical-scavenging activity.** The ABTS free radical scavenging ability of the samples was determined using the method reported previously with some modifications.<sup>29</sup> ABTS radical cation was produced by ABTS solution (7 mmol L<sup>-1</sup>) with 2.5 mmol L<sup>-1</sup> potassium persulfate, and the mixture was stored in the dark at 26 °C for 16 h. The ABTS free radical solution was diluted with water to an absorbance of approximately 0.70 at 734 nm, which was the ABTS working solution. 150  $\mu\text{L}$  of each sample (final concentration 20–100  $\mu\text{g mL}^{-1}$ ) in methanol and 150  $\mu\text{L}$  of ABTS working solution were mixed in a test tube reacting at room temperature in the dark for 15 min. After the reaction, the absorbance was measured at a wavelength of 734 nm.

### Anticancer assay

Human pulmonary carcinoma cells (A549) and human hepatocellular carcinoma cells (HepG2) were cultured in DMEM supplemented with 10% FBS and 1% antibiotics at 37 °C in a 5% (v/v) CO<sub>2</sub> atmosphere. Then, the cells were seeded and incubated in 96-well plates with  $2.0 \times 10^4$  cells per well for 24 h. They were then treated with various concentrations of Phl, Inz,

and Phl–Inz cocrystals (20, 40, 80, 160, and 320  $\mu\text{mol L}^{-1}$ ) for 24 h, for which 5 replicates and a blank control group were set up concurrently. The samples were dissolved in DMSO attenuated to a specific concentration by adding DMEM. After 24 h, the supernatant was removed, and the cells were incubated with 20  $\mu\text{L}$  MTT (5 mg mL<sup>-1</sup>) for 4 h at 37 °C. After discarding the supernatant, 150  $\mu\text{L}$  of DMSO was added per hole, and absorbance values were measured at 570 nm using a microplate reader.

## Results and discussion

### Cocrystal screening by PXRD

Phloretin had characteristic peaks at 6.9°, 9.4°, 13.8°, 16.4°, 17.7°, 27.0°, and 27.9° (Fig. 2a). These characteristic peaks of phloretin were also found in phloretin–theophylline, phloretin–benzamide, phloretin–maleic acid, phloretin–proline, phloretin–nicotinic acid and phloretin–isonicotinic acid (Fig. 2b–g), which showed that the phloretin did not form cocrystal with these co-formers by applying the solvent evaporation method at a ratio of 1 : 1 in methanol. As illustrated in Fig. 2h, the PXRD pattern of phloretin–picolinic acid showed that the characteristic peaks of phloretin at 6.9°, 9.4°, 13.8° and 16.4° disappeared. Moreover, characteristic peaks of phloretin (6.9°, 9.4°, 13.8° and 16.4°) disappeared from the PXRD pattern of phloretin–isoniazid (Fig. 2i). These phenomena indicate the formation of new crystalline phases. To further determine whether phloretin forms cocrystal with picolinic acid and isoniazid, samples of phloretin–picolinic acid (Phl–Pa) and phloretin–isoniazid (Phl–Inz) were tested using DSC-TG.

### Thermal analysis

The thermal analysis method can be used to check the purity of the crystalline phases.<sup>20,30</sup> The thermal behaviours of crystals can be determined by differential scanning calorimetry (DSC) and thermogravimetric analysis (TG).<sup>31,32</sup> In the thermogram (Fig. 3), 266.9 °C, 169.6 °C and 137.1 °C in DSC endotherms were the melting points of phloretin, isoniazid and picolinic acid, respectively. The cocrystal Phl–Inz exhibited the formation of a sharp endothermic peak at 182.7 °C (Fig. 3). The position of the endothermic peak of Phl–Inz was different from that of Phl and Inz, which showed that the peak was the melting point of the cocrystal. The appearance of a new single peak illustrated the formation of a new crystal with high crystallinity and purity. Furthermore, the results of the TGA showed that the Phl–Inz cocrystal had approximately a 7.9% weight loss at about 219 °C. This phenomenon means the decomposition of the Phl–Inz cocrystal with the loss of –NH–NH<sub>2</sub>. However, the mixture of Phl–Pa exhibited two sharp endothermic peaks at 224.5 °C and 261.8 °C. The position of the endothermic peak of the Phl–Pa mixture at 261.8 °C was similar to the melting point of phloretin, and the peak of the Phl–Pa mixture at 224.5 °C was different from the melting points of phloretin and picolinic acid. These two endothermic peaks showed that the new crystalline phase was formed in the phloretin and picolinic acid by applying the solvent evaporation method, but some phloretins



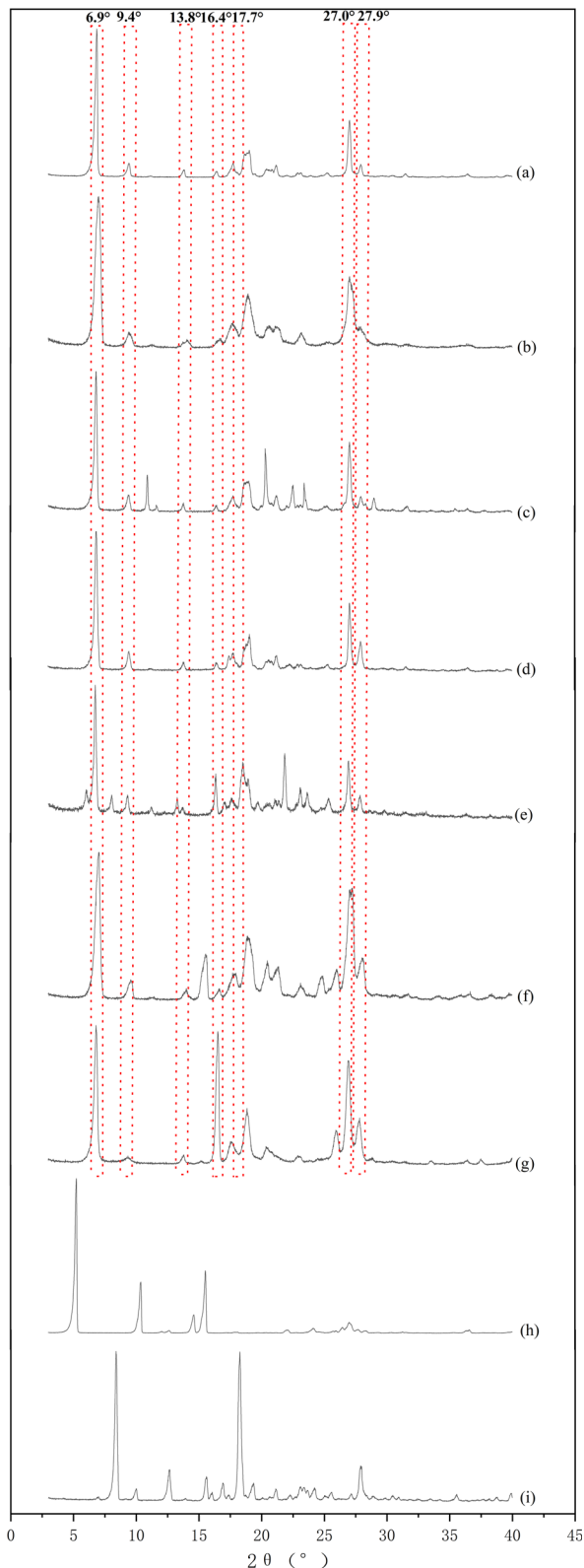


Fig. 2 PXRD patterns of Phl and co-formers.

were still in a free state, which explicates that the mixture includes a new crystal and phloretin monomer. Based on the analysis of DSC-TG, pure Phl-Inz cocrystal was successfully

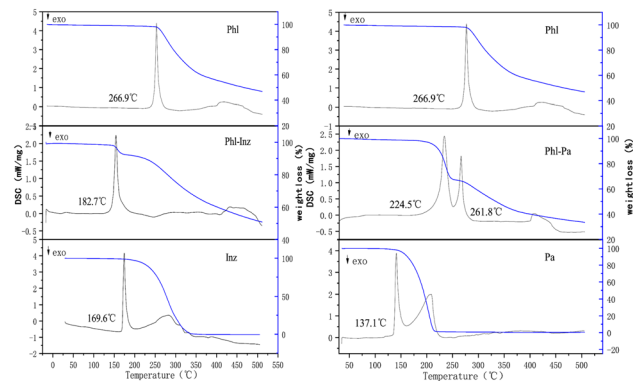


Fig. 3 The DSC and TG curves.

formed by the solvent evaporation method, but pure Phl-Pa cocrystal failed. However, DSC-TG can only provide thermodynamic information about the cocrystal. More characterization methods (including FT-IR, HNMR, PXRD and SCXRD) were needed to determine the structure of the cocrystal.

#### FT-IR analysis

The energy absorbed or scattered by the bonds in the cocrystal differs from the energy of the pure components. The formation of cocrystals could lead to changes in positions, shape and intensity of absorption pattern.<sup>33,34</sup> Infrared spectroscopy can help to obtain more information about the intermolecular interactions of functional groups involved in their vibrational frequency changes. For Phl (Fig. 4), the characteristic peaks appeared at  $3210\text{ cm}^{-1}$  and  $1633\text{ cm}^{-1}$ , which corresponded to the O-H and C=O stretching vibrations of the hydroxyl groups and carbonyl groups. The infrared spectrum of Inz reflected the characteristic peaks that appeared at  $3303\text{ cm}^{-1}$ ,  $3171\text{ cm}^{-1}$  and  $3106\text{ cm}^{-1}$  corresponding to N-H of the hydrazide groups. The

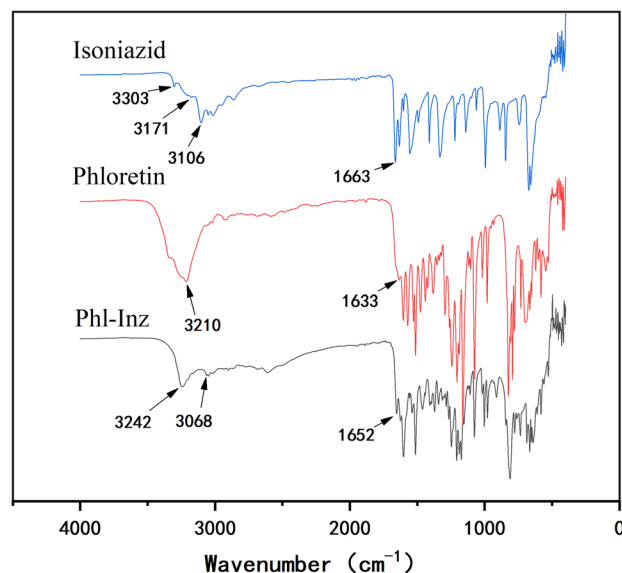


Fig. 4 IR of Phl, Inz and Phl-Inz.



characteristic peak located at  $1663\text{ cm}^{-1}$  corresponds to the C=O stretching vibrations of the carbonyl group. The hydrogen bonding between Phl and Inz in the cocrystal led to a change in the position of the vibrational frequencies, which differed from Phl and Inz. The vibrational frequency of O–H of Phl shifted to  $3242\text{ cm}^{-1}$  from  $3210\text{ cm}^{-1}$ , while that of N–H of Inz shifted to  $3068\text{ cm}^{-1}$  from  $3106\text{ cm}^{-1}$ . The C=O of Phl and Inz moved from  $1633\text{ cm}^{-1}$  and  $1663\text{ cm}^{-1}$  to  $1652\text{ cm}^{-1}$ , respectively. The formation of hydrogen bonding in the Phl–Inz cocrystal results in a blue shift or red shift of the stretching vibrations.<sup>35–37</sup>

### <sup>1</sup>H NMR analysis

The ratio of Phl and Inz in the cocrystal was identified with <sup>1</sup>H NMR. In Fig. 5, the characteristic peaks of the chemical shift of Phl in <sup>1</sup>H NMR (DMSO-*d*<sub>6</sub>) spectrum were as follows (red points in Fig. 5):  $\delta$ 12.24 (s, 2H), 10.35 (s, 1H), 9.14 (s, 1H), 7.02 (d,  $J = 8.4\text{ Hz}$ , 2H), 6.67 (d,  $J = 8.4\text{ Hz}$ , 2H), 5.82 (s, 2H), 3.22 (t,  $J = 7.8\text{ Hz}$ , 2H), and 2.77 (t,  $J = 7.8\text{ Hz}$ , 2H). For Inz, <sup>1</sup>H NMR (DMSO-*d*<sub>6</sub>) spectrum was as follows (green points in Fig. 5):  $\delta$ 10.10 (s, 1H), 8.71 (d,  $J = 6.1\text{ Hz}$ , 2H), 7.73 (d,  $J = 6.1\text{ Hz}$ , 2H), and 4.63 (s, 2H). The stoichiometric ratio of Phl and Inz is 1 : 1 from the ratio of the integration results of the characteristic peaks of Phl and Inz in the <sup>1</sup>H NMR spectrum.

### PXRD analysis

Different crystal phases of a substance can be obtained by applying the powder X-ray diffraction method to obtain different diffraction patterns, which is a common method for the characterization of cocrystals.<sup>38</sup> Fig. 6 shows the diffraction patterns of Phl, Inz and cocrystal. Phl exhibited characteristic diffraction peaks at  $6.9^\circ$ ,  $9.4^\circ$ ,  $13.8^\circ$ ,  $16.4^\circ$ ,  $17.7^\circ$ ,  $27.0^\circ$ , and  $27.9^\circ$ . The characteristic diffraction peaks of Inz were  $9.7^\circ$ ,  $11.9^\circ$ ,  $14.2^\circ$ ,  $15.4^\circ$ ,  $16.6^\circ$ ,  $19.6^\circ$ ,  $24.0^\circ$ ,  $25.3^\circ$ ,  $28.7^\circ$ , and  $32.0^\circ$ . The PXRD analysis of Phl–Inz exhibited new characteristic reflections at  $8.3^\circ$ ,  $12.6^\circ$ , and  $18.2^\circ$  positions ( $2\theta$ ), which differed from those in Phl and Inz. The existence of new phases from Phl and Inz was confirmed by PXRD. The diffraction peaks shown in the simulated diffraction pattern of a single crystal are approximately the same as those of a cocrystal.

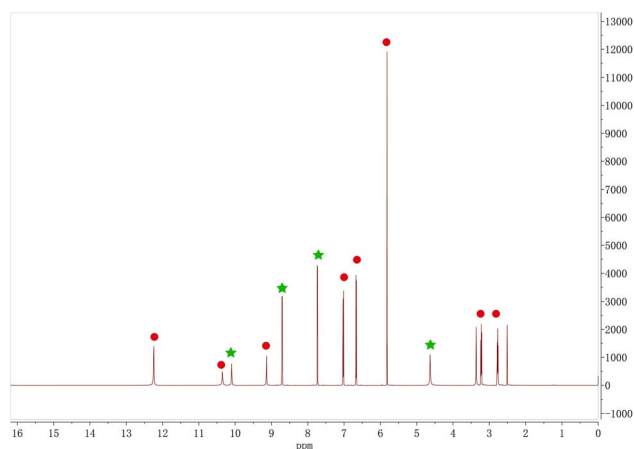


Fig. 5 <sup>1</sup>H NMR of Phl–Inz cocrystal.

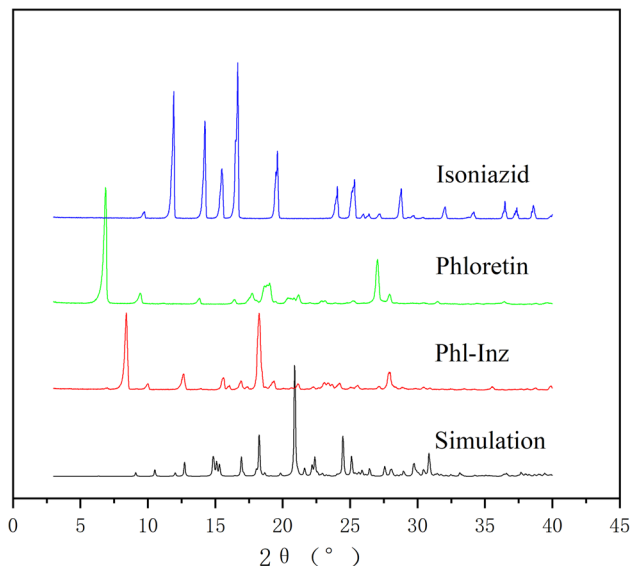


Fig. 6 PXRD patterns of Phl–Inz cocrystal.

### Crystal structure analysis

SCXRD can obtain microscopic information, such as space group, unit cell, bond length, bond angle and intermolecular interaction, by measuring the structure of a single crystal.<sup>39</sup> Many relevant isoniazid-based cocrystals have been reported.<sup>39–44</sup> The structure of Phl–Inz crystallized in the triclinic space group  $P\bar{1}$  (Table 1), with two molecules of Phl and Inz in the asymmetric unit. A unit cell contains two asymmetric units. One molecule of Phl connected with Inz through O1–H1...N1 or O6–H6A...N4 to form a dimer. The two dimers were further linked by O5–H5...O1 or O10–H10...O6 hydrogen bond between the hydroxy groups of the adjacent Phl molecules to form a tetramer. The tetramers were further connected by O4–H4...N3 and N1–H1A...O2 hydrogen bonds or O9–H9...N6 and N4–H4A...O7 to form 2D structure of the cocrystal (Fig. 7c and d). The 2D structures are connected by N2–H2A...O12 and N5–H5B...O11 hydrogen bonds to form 3D structures (Fig. 7e). The hydrogen-bonding distances and angles for the Phl–Inz cocrystal were showed in Table 2.

### Hirshfeld surface analysis

To have a broader view of the packing modes and interactions between the components in the cocrystal, the Hirshfeld surface could be examined in a visual way.<sup>45</sup> Hirshfeld surface (HS) and 2D fingerprint plots were prepared using Crystal Explorer 21.5. As shown in Fig. 8, HS of Phl–Inz revealed the interaction in O–H...O and O–H...N shown in bright red on the surface, while H...H contact was exhibited in the blue areas on the surface. Based on the finger plots of cocrystal (Fig. 8), the contacts of H...H, H...C/C...H, H...O/O...H and H...N/N...H accounted for 40.1%, 20.5%, 25.8% and 7.4% of HS, respectively. H...H interaction contributed the most to the total HS of Phl–Inz, indicating that the cocrystal structure is loose, which creates favourable conditions for regulating the solubility of Phl. The



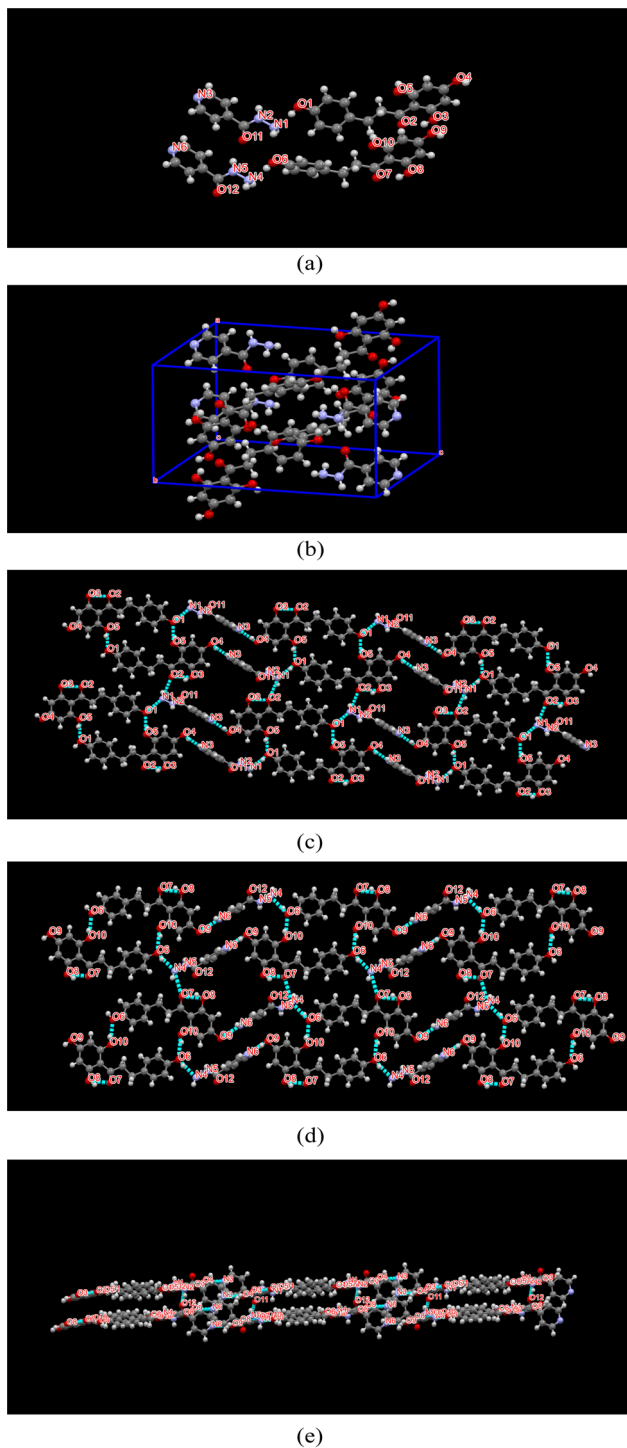


Fig. 7 (a) Asymmetric unit, (b) cell packing, (c) 2D structure, (d) 3D sheet structure of PhI-Inz cocrystal. H-bonds are represented by dashed lines.

cocrystal structure was stable in space through hydrogen bonding and van der Waals forces.

### Analysis of solubility experiments

The purpose of these experiments was to modify the physico-chemical properties of PhI using cocrystals to improve its poor

Table 1 Crystallographic data and structure refinement parameters for the PhI-Inz cocrystal

Compound	PhI-Inz
Empirical formula	C <sub>21</sub> H <sub>21</sub> N <sub>3</sub> O <sub>6</sub>
Formula weight	411.41
Temperature (K)	150(10)
$\lambda$ (Å)	1.54184
Crystal size (mm <sup>3</sup> )	0.29 × 0.15 × 0.03
Space group	$P\bar{1}$
Crystal system	Triclinic
<i>a</i> (Å)	9.8309(4)
<i>b</i> (Å)	9.8954(4)
<i>c</i> (Å)	20.6193(7)
$\alpha$ (°)	92.308(3)
$\beta$ (°)	91.398(3)
$\gamma$ (°)	107.015(3)
Volume (Å <sup>3</sup> )	1915.13(12)
<i>Z</i>	4
$\rho_{\text{calc}}$ (g cm <sup>-3</sup> )	1.427
$\mu$ (mm <sup>-1</sup> )	0.887
2 $\theta$ range	8.59–149.404
<i>F</i> (000)	864
Index ranges	–12 ≤ <i>h</i> ≤ 11 –12 ≤ <i>k</i> ≤ 12 –25 ≤ <i>l</i> ≤ 25
Reflections collected	30 217
Independent reflections	7393 [ <i>R</i> <sub>int</sub> = 0.0329, <i>R</i> <sub>sigma</sub> = 0.0218]
Data/restraints/parameters	7393/0/550
GOF	1.044
Final <i>R</i> indexes [ <i>I</i> ≥ 2 $\sigma$ ( <i>I</i> )]	0.0878/0.2537
Final <i>R</i> indexes (all data)	0.0932/0.2574
Largest diff. peak/hole (e Å <sup>-3</sup> )	0.54/–0.36

Table 2 Hydrogen-bonding distances and angles for the PhI-Inz cocrystal<sup>a</sup>

Hydrogen bond	H...A (Å)	D...A (Å)	$\angle$ D–H...A (°)
O1–H1...N1	1.91	2.736(4)	169.9
O1–H1...N2	2.73	3.418(4)	140.8
O3–H3...O2	1.76	2.504(3)	147.1
O4–H4...N3 <sup>1</sup>	1.94	2.750(4)	160.8
O5–H5...O1 <sup>2</sup>	1.87	2.677(3)	159.8
C6–H6...O5 <sup>2</sup>	2.88	3.474(4)	121.5
C12–H12...N3 <sup>1</sup>	2.80	3.456(5)	127.3
O6–H6A...N4	1.92	2.751(4)	168.0
O6–H6A...N5	2.78	3.492(4)	143.5
O8–H8...O7	1.76	2.505(3)	147.3
O9–H9...N6 <sup>1</sup>	1.95	2.753(4)	159.9
O10–H10...O6 <sup>3</sup>	1.85	2.664(3)	163.3
C27–H27...N6 <sup>1</sup>	2.77	3.431(4)	127.7
N1–H1A...O2 <sup>4</sup>	2.21	2.986(4)	146.8
N2–H2A...O8 <sup>4</sup>	2.77	3.330(4)	122.8
N2–H2A...O12 <sup>5</sup>	1.98	2.784(4)	151.9
C33–H33...O8 <sup>4</sup>	2.47	3.406(4)	169.9
N4–H4A...O7 <sup>6</sup>	2.29	2.961(4)	132.1
N4–H4B...O1 <sup>7</sup>	2.47	3.250(4)	151.6
N5–H5B...O3 <sup>4</sup>	2.70	3.270(4)	123.3
N5–H5B...O11	1.99	2.773(4)	148.3
C39–H39...O3 <sup>4</sup>	2.46	3.402(4)	169.5

<sup>a</sup> Symmetry codes: <sup>1</sup>1 + *X*, +*Y*, 1 + *Z*; <sup>2</sup>2 – *X*, 1 – *Y*, 1 – *Z*; <sup>3</sup>3 – *X*, 1 – *Y*, 1 – *Z*; <sup>4</sup>4 – *X*, –*Y*, 1 – *Z*; <sup>5</sup>5 1 + *X*, +*Y*, +*Z*; <sup>6</sup>6 – *X*, –*Y*, 1 – *Z*; <sup>7</sup>7 – 1 + *X*, +*Y*, +*Z*.



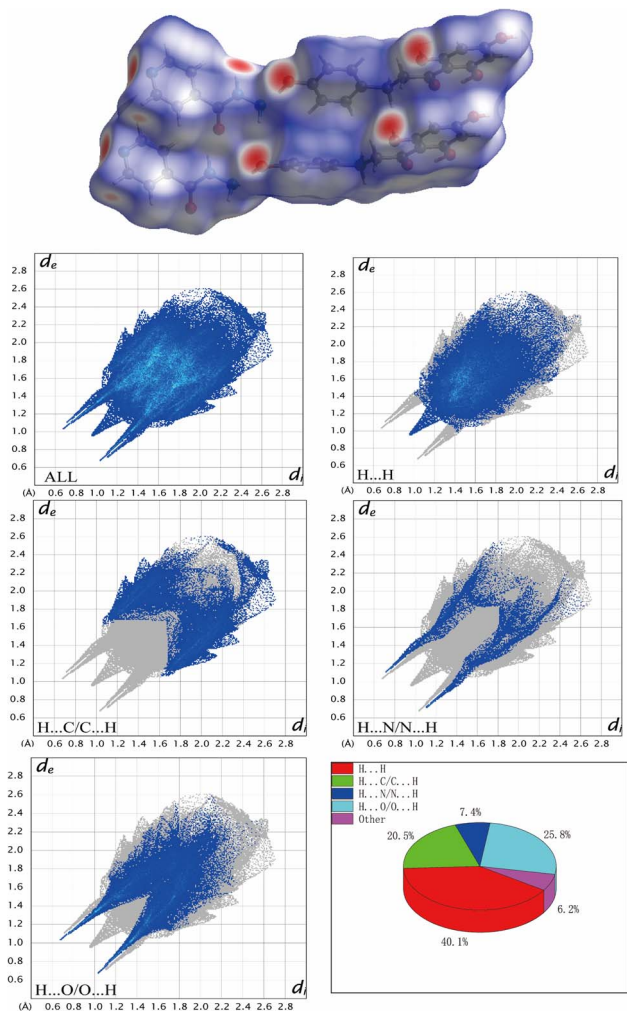


Fig. 8 Hirshfeld surface and 2D fingerprint plots of Phl–Inz.

water solubility. The results of solubility experiments on the Phl–Inz cocrystal in pH 1.2 and pH 6.8 fluid at various times are presented in Fig. 9. The equilibrium solubility of pure Phl was around  $4.38 \mu\text{g mL}^{-1}$  (pH 1.2) and  $21.39 \mu\text{g mL}^{-1}$  (pH 6.8). The solubility of Phl in the mixture with Inz did not improve (Fig. 9a and b). After the formation of the Phl–Inz cocrystal, the solubility of cocrystal in two buffers distinctly increased to  $46.84 \mu\text{g mL}^{-1}$  (pH 1.2) at 30 min and  $477.24 \mu\text{g mL}^{-1}$  (pH 6.8) at 15 min. Phl's concentration increased to the maximum value and then began to decrease within 40 min, but the equilibrium solubility was still higher than the levels exhibited by pure Phl. This may be because Inz molecules with better water solubility dissolved first in the initial phase of dissolution, leading to the destruction of the molecular spatial structure and the rapid dissolution of Phl molecules to supersaturation. The recrystallization of supersaturated Phl results in the decreased solubility of Phl.

The remaining samples were tested by PXRD after the solubility experiment. The results of PXRD patterns (Fig. 9c) showed that the remaining materials had a few characteristic peaks of the Phl–Inz cocrystal, such as  $8.3^\circ$ ,  $12.6^\circ$  and  $18.2^\circ$  (with star symbol). However, the characteristic of raw Phl at  $6.9^\circ$  was

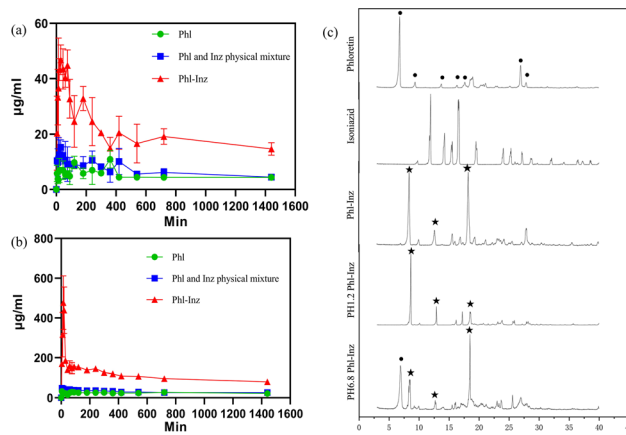


Fig. 9 The powder dissolution curve of Phl, Inz and Phl–Inz cocrystal ((a) pH = 1.2), (b) pH = 6.8). (c) PXRD patterns of samples after testing.

found in the PXRD pattern of the cocrystal (pH 6.8). At pH 6.8, the solubility of the cocrystal decreased abruptly but decreased gradually at pH 1.2. The reason may be that the solubility of Phl at pH 6.8 is higher than that of pH 1.2, and the solubility of Phl in a short time is also higher than that of pH 1.2 owing to the influence of the rapid dissolution of Inz. More free Phl is more likely to recrystallize at pH 6.8 than at pH 1.2, so the solubility of the cocrystal at pH 6.8 decreases rapidly. The phenomenon explained that the Phl–Inz cocrystal dissolves into the individual molecules in the solute and is recrystallized because of poor solubility. The phenomenon showed a change in Phl solubility owing to the formation of a new crystalline phase.

#### Analysis of simulated digestion *in vitro*

The release profile of free phloretin and phloretin in cocrystal tested *in vitro* simulated gastrointestinal digestion experiment is shown in Fig. 10 throughout the entire 6 h in SGF and SIF fluid. Approximately 11% free phloretin diffused to the SGF, followed by another approximately 7% released in the SIF, totalling the 18% cumulative release at the end of the experiment. In contrast, there was around 16% phloretin in the cocrystal released in the SGF and another 15% released in the SIF, totalling 31% cumulative release in the release medium. During the incubation of intestinal digestion, it was shown that the release of phloretin in the cocrystal was better than that of the free phloretin. It could correspond to the results of the solubility experiments that the solubility of Phl–Inz cocrystal is better than pure Phl.

#### Analysis of *in vitro* antioxidant activity

The *in vitro* antioxidant activity of Phl–Inz cocrystal, Phl and Inz was evaluated with DPPH and ABTS free radical scavenging rate<sup>46</sup> (Fig. 11a and b). In the concentration range of  $20\text{--}100 \mu\text{g mL}^{-1}$ , the DPPH free radical scavenging rate of the compounds increased as the mass concentration increased. When the mass concentration was  $100 \mu\text{g mL}^{-1}$ , the DPPH free radical scavenging rate of Phl–Inz reached 88.7%, while that of pure Phl was



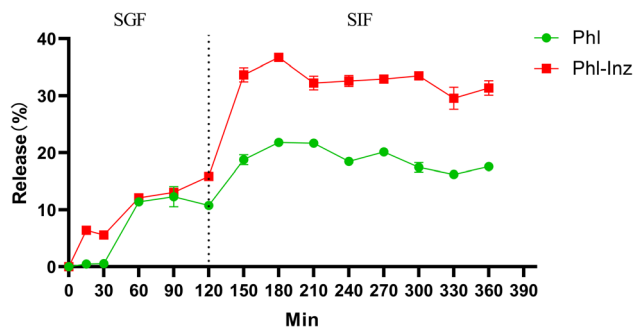


Fig. 10 Release properties of phloretin from free phloretin and Phl-Inz cocystal during an *in vitro* digestion study.

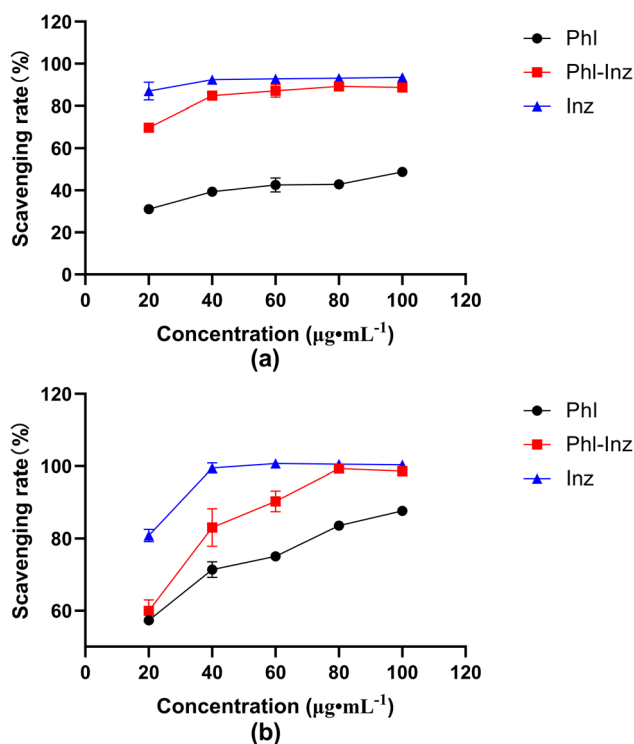


Fig. 11 Free radical scavenging activity of Phl, Inz and Phl-Inz cocystal (a) DPPH; (b) ABTS).

48.8%. The concentration of Phl, Inz and cocystals positively correlated with ABTS free radical scavenging rate in the range of 20–100  $\mu\text{g mL}^{-1}$ . The ABTS free radical scavenging rate of Phl-Inz reached 98.6% in 100  $\mu\text{g mL}^{-1}$  while that of pure Phl was 87.7%. The results indicated that the DPPH and ABTS radical scavenging activity of Phl-Inz had nearly 82% and 12% enhancement over that shown by pure Phl.

#### Anticancer evaluation

To further ascertain whether the improved physicochemical properties can promote the enhancement of antitumor activities, we used various concentrations of Phl and cocystal to incubate cancer cells and investigate their effects on cancer cell proliferation (Fig. 12a and b). The results showed that cocystal

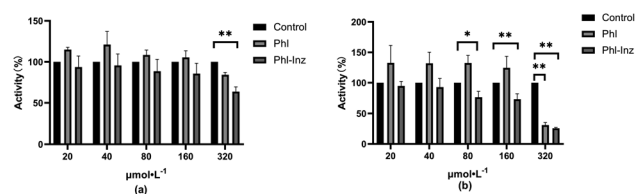


Fig. 12 The cytotoxicity of Phl and cocystal against the tested cancer cells (a) A549 cell; (b) HepG2).

exhibited an inhibitory effect on the proliferation of A549 cells at 320  $\mu\text{mol L}^{-1}$  ( $P < 0.01$ ) and better than the effect of Phl, but other concentrations had insignificant inhibitory effects. For the result of HepG2, cocystal showed significant inhibitory effects at 80  $\mu\text{mol L}^{-1}$ , 160  $\mu\text{mol L}^{-1}$  and 320  $\mu\text{mol L}^{-1}$  ( $P < 0.01$ , 0.05) but Phl was only at 320  $\mu\text{mol L}^{-1}$ . The improved inhibitory ability may be basically due to the cocystal having better physicochemical properties after Phl forming cocystal with Inz. The better solubility of the cocystal can facilitate the dissolution of Phl at a faster rate, thereby inducing high-concentration drug enrichment around the cancer cells, which provides sufficient conditions for sustained efficacy.

## Conclusions

In this study, we selected several CCFs and tried to form cocystals with Phl by applying the solvent evaporation method. Based on the results of PXRD and DSC-TG, it was determined that only Phl formed a cocystal with Inz. Fourier-transform infrared was used to determine the hydrogen bonding between the hydroxyl group in Phl and the hydrazide group in Inz. Single-crystal diffraction and  $^1\text{H}$  NMR showed that the stoichiometric ratio of the two components in the crystal was 1 : 1. Phl and Inz were bound to each other through various hydrogen bonds in the cocystal. The Hirshfeld surface and 2D fingerprint plots further elucidate the intermolecular interaction of the two components in the cocystal. The solubility experiment showed that the *in vitro* dissolution rate and equilibrium solubility of the Phl-Inz cocystal were better than those of pure Phl. The release of phloretin in the cocystal was better than that of pure phloretin in the gastrointestinal fluid. Moreover, *in vitro* antioxidant activity and anti-cancer activity of cocystals increased. The above work showed a promising approach to overcoming the poor physicochemical properties of parent drugs by forming cocystal structures, and pharmaceutical cocystals could be used as an effective technology for developing new drugs.

## Author contributions

Zhongyu Lu: data curation, formal analysis, investigation, visualization, and writing-original draft. Hankun Chen: supervision and editing. Jiaxin Mo: formal analysis and validation. Xiaohong Yuan: investigation and formal analysis. Dawei Wang: formal analysis; Xianhui Zheng: formal analysis; Wei Zhu: supervision, resources, and funding acquisition.



## Conflicts of interest

There are no conflicts to declare.

## Acknowledgements

This research was funded by Guangdong Provincial Hospital of Chinese Medicine Science and Technology Research Program (YN2019MJ11); Scientific Research Project of Guangdong Administration of Traditional Chinese Medicine (202231144); Foundation of Guangzhou Science and Technology Bureau (202201020296), and the Foshan Project of Key Areas of Science and Technology Research (2120001008478).

## Notes and references

- R. L. Birru, K. Bein, H. Wells, N. Bondarchuk, A. Barchowsky, Y. P. Di and G. D. Leikauf, *Mol. Nutr. Food Res.*, 2021, **65**, e2000658.
- L. Wang, Z. W. Li, W. Zhang, R. Xu, F. Gao, Y. F. Liu and Y. J. Li, *Molecules*, 2014, **19**, 16447–16457.
- X. Li, B. Chen, H. Xie, Y. He, D. Zhong and D. Chen, *Molecules*, 2018, **23**, 1162.
- X. Y. Lu, Y. Y. Zeng, Y. X. Ye, Y. Y. Zhou, J. J. Mu and X. H. Zhao, *Yaoxue Xuebao*, 2009, **44**, 480–485.
- D. Barreca, E. Bellocco, G. Lagana, G. Ginestra and C. Bisignano, *Food Chem.*, 2014, **160**, 292–297.
- B. Y. Choi, *Molecules*, 2019, **24**, 278.
- S. Huang, J. Xu, Y. Peng, M. Guo and T. Cai, *Cryst. Growth Des.*, 2019, **19**, 6837–6844.
- L. Gu, R. Sun, W. Wang and Q. Xia, *Chem. Phys. Lipids*, 2022, **242**, 105150.
- T. P. Anunciato Casarini, L. A. Frank, A. R. Pohlmann and S. S. Guterres, *Eur. J. Pharmacol.*, 2020, **889**, 173593.
- A. Karagianni, M. Malamataris and K. Kachrimanis, *Pharmaceutics*, 2018, **10**, 18.
- G. Kuminek, F. Cao, A. Bahia de Oliveira da Rocha, S. Goncalves Cardoso and N. Rodriguez-Hornedo, *Adv. Drug Delivery Rev.*, 2016, **101**, 143–166.
- J. Varshosaz, E. Ghassami and S. Ahmadipour, *Curr. Pharm. Des.*, 2010, **24**, 2473–2496.
- D. Srivastava, Z. Fatima, C. D. Kaur, S. L. Tulsankar, S. S. Nashik and D. A. Rizvi, *Recent Pat. Drug Delivery Formulation*, 2019, **13**, 62–69.
- I. Sathisaran and S. V. Dalvi, *Pharmaceutics*, 2018, **10**, 108.
- N. Schultheiss and A. Newman, *Cryst. Growth Des.*, 2009, **9**, 2950–2967.
- W. Li, J. Pi, Y. Zhang, X. Ma, B. Zhang, S. Wang, D. Qi, N. Li, P. Guo and Z. Liu, *Fitoterapia*, 2018, **129**, 85–93.
- M. Liu, C. Hong, Y. Yao, H. Shen, G. Ji, G. Li and Y. Xie, *Eur. J. Pharm. Biopharm.*, 2016, **107**, 151–159.
- M. Rodrigues, B. Baptista, J. A. Lopes and M. C. Sarraguca, *Int. J. Pharm.*, 2018, **547**, 404–420.
- I. Miroshnyk, S. Mirza and N. Sandler, *Expert Opin. Drug Delivery*, 2009, **6**, 333–341.
- N. Qiao, M. Li, W. Schlindwein, N. Malek, A. Davies and G. Trappitt, *Int. J. Pharm.*, 2011, **419**, 1–11.
- Y. Liu, F. Yang, X. Zhao, S. Wang, Q. Yang and X. Zhang, *Pharmaceutics*, 2022, **14**, 94.
- J. Xu, Y. Huang, S. Ruan, Z. Chi, K. Qin, B. Cai and T. Cai, *CrystEngComm*, 2016, **18**, 8776–8786.
- Z. Zhang, D. Li, C. Luo, C. Huang, R. Qiu, Z. Deng and H. Zhang, *Cryst. Growth Des.*, 2019, **19**, 3851–3859.
- Z. Zhou, W. Li, W. J. Sun, T. Lu, H. H. Y. Tong, C. C. Sun and Y. Zheng, *Int. J. Pharm.*, 2016, **509**, 391–399.
- G. M. Sheldrick, *Acta Crystallogr., Sect. A: Found. Adv.*, 2015, **71**, 3–8.
- G. M. Sheldrick, *Acta Crystallogr., Sect. C: Struct. Chem.*, 2015, **71**, 3–8.
- P. R. Spackman, M. J. Turner, J. J. McKinnon, S. K. Wolff, D. J. Grimwood, D. Jayatilaka and M. A. Spackman, *J. Appl. Crystallogr.*, 2021, **54**, 1006–1011.
- P. P. Wang, Z. G. Luo and X. C. Peng, *J. Agric. Food Chem.*, 2018, **66**, 10598–10607.
- P. Rozi, A. Abuduwaili, P. Mutailifu, Y. Gao, R. Rakhmanberdieva, H. A. Aisa and A. Yili, *Int. J. Biol. Macromol.*, 2019, **131**, 97–106.
- A. Raheem Thayyil, T. Juturu, S. Nayak and S. Kamath, *Adv. Pharm. Bull.*, 2020, **10**, 203–212.
- Z. Zhou, H. M. Chan, H. H. Sung, H. H. Tong and Y. Zheng, *Pharm. Res.*, 2016, **33**, 1030–1039.
- I. Nugrahani, D. Utami, Y. P. Nugraha, H. Uekusa, R. Hasianna and A. A. Darusman, *Heliyon*, 2019, **5**, e02946.
- S. Sawatdee, A. Atipairin, S. Rakkummerd, O. Suriyaphol, D. J. Harding, P. Muenraya and P. Harding, *J. Adv. Pharm. Technol. Res.*, 2021, **12**, 408–419.
- P. Cerreia Vioglio, M. R. Chierotti and R. Gobetto, *Adv. Drug Delivery Rev.*, 2017, **117**, 86–110.
- R. Chadha, Y. Bhalla, A. Nandan, K. Chadha and M. Karan, *J. Pharm. Biomed. Anal.*, 2017, **134**, 361–371.
- A. Sokal, E. Pindelska, L. Szeleszczuk and W. Kolodziejcki, *Int. J. Pharm.*, 2017, **522**, 80–89.
- Z. Zhou, W. Li, W.-J. Sun, T. Lu, H. H. Y. Tong, C. C. Sun and Y. Zheng, *Int. J. Pharm.*, 2016, **509**, 391–399.
- E. Pindelska, A. Sokal and W. Kolodziejcki, *Adv. Drug Delivery Rev.*, 2017, **117**, 111–146.
- K. K. Bisht, P. Patel, Y. Rachuri and S. Eringathodi, *Acta Crystallogr., Sect. B: Struct. Sci., Cryst. Eng. Mater.*, 2014, **70**, 63–71.
- P. Grobelny, A. Mukherjee and G. R. Desiraju, *CrystEngComm*, 2011, **13**, 4358–4364.
- R. Kaur, S. S. R. R. Perumal, A. J. Bhattacharyya, S. Yashonath and T. N. Guru Row, *Cryst. Growth Des.*, 2014, **14**, 423–426.
- I. Sarcevic, L. Orola, M. V. Veidis, A. Podjava and S. Belyakov, *Cryst. Growth Des.*, 2013, **13**, 1082–1090.
- M. C. Scheepers and A. Lemmerer, *Acta Crystallogr., Sect. B: Struct. Sci., Cryst. Eng. Mater.*, 2022, **78**, 857–867.
- B. Swapna, D. Maddileti and A. Nangia, *Cryst. Growth Des.*, 2014, **14**, 5991–6005.
- M. A. Spackman and D. Jayatilaka, *CrystEngComm*, 2009, **11**, 19–32.
- I. G. Munteanu and C. Apetrei, *Int. J. Mol. Sci.*, 2021, **22**, 3380.

